American Mineralogist, Volume 86, pages 1358–1366, 2001

Evidence for an *I*2/*a* to *Imab* phase transition in the silica polymorph moganite at ~570 K

PETER J. HEANEY[1,*] AND JEFFREY E. POST[2]

[1]Department of Geosciences, 309 Deike, Penn State University, University Park, Pennsylania 16802, U.S.A.
[2]Department of Mineral Sciences, National Museum of Natural History, Smithsonian Institution, Washington, D.C. 20560-0119, U.S.A.

ABSTRACT

Rietveld analysis of synchrotron X-ray powder diffraction data for the silica mineral moganite from 100 K to 1354 K has revealed a reversible phase transition from space group *I*2/*a* to *Imab* at approximately 570 K. The thermal expansion behavior of the lattice parameters alters sharply at the transition point, and the monoclinic β angle decreases to 90°. The displacive transition from α- to β-moganite is effected by the rotation of apparently rigid tetrahedra about the [010] axis, and the linear temperature dependence of the volume strain and of the non-symmetry-breaking e_{11} and e_{22} strains indicates that the character of the transition is second-order. The continuous increase in the **b** axis over the entire temperature range reveals a concomitant rotation of tetrahedra about [100] that does not affect the overall symmetry. In addition, we present a refinement without structural constraints for α-moganite at room temperature using time-of-flight neutron diffraction data.

INTRODUCTION

The silica minerals have yielded some of our most profound insights into the mechanisms that drive displacive phase transitions in solid materials. The chemical simplicity of the system allows an unfettered examination of the interaction between structure and transition behavior, and the full polymerization of the silica network promotes a long-range coupling between the order parameter and the spontaneous strain. This interaction generates a rich diversity of transition behaviors in silica minerals, which have served as models for the complex transformation processes that attend temperature and pressure variations in a multiplicity of mineral classes. Soft modes, for example, were first discovered during C.V. Raman's investigations of the α-β quartz transition (Raman and Nedungadi 1940), and the silica polymorphs have played an important role in the development of the rigid unit mode (RUM) theory of phase transitions (Dove et al. 2000). Consequently, scientists have extensively documented the displacive transformations that occur in the low-pressure polymorphs quartz, tridymite, and cristobalite (reviewed in Heaney 1994). In this paper, we present evidence for a structural transition in the fourth species of crystalline silica common in crustal environments—the mineral moganite.

Despite initial skepticism regarding the distinction between moganite and quartz, the International Commission on New Minerals and Mineral Names approved moganite as a mineral species in 1999. First described from chert-like nodules within rhyolitic ignimbrites of the Mogán Formation, Gran Canaria, Spain (Flörke et al. 1976, 1984), moganite apparently lacks a stability field in the pure SiO_2 system. Although some molecular dynamical simulations have suggested that moganite is more stable than quartz at ambient conditions (Murashov and Svishchev 1998), calorimetric studies yield an enthalpy for moganite relative to quartz at 298 K of 3.4 ± 0.7 kJ/mol, slightly higher than those of tridymite and cristobalite (Petrovic et al. 1996). To date, no one has reported a procedure for the synthesis of moganite.

Moganite is a widespread and significant indicator mineral. Heaney and Post (1992) have demonstrated that moganite is extensively intergrown with quartz in microcrystalline silica varieties that are less than ~100 Ma in age. Over longer time scales it diagenetically transforms to quartz. Moganite appears to precipitate most readily from alkaline brines, and high concentrations (>20 wt%) of moganite in chert signify formation in evaporitic paleo-environments (Heaney 1995). Gíslason et al. (1997) have shown that the solubility of moganite (44 mg/kg) is significantly greater than that of quartz (6 mg/kg). Consequently, geothermometers for hydrothermal fluids that are based on the concentration of dissolved silica (Fournier and Rowe 1966; Fournier 1977) must account for the presence of moganite within the chalcedony that co-exists with the solution.

The structure of moganite (Miehe et al. 1988; Miehe and Graetsch 1992) can be visualized as quartz that is Brazil twinned along (101) at the unit-cell scale: right-handed slabs of quartz alternate regularly with left-handed slabs to generate a structure that is distinct from quartz (Fig. 1). Miehe and Graetsch (1992) refined the structure in the non-conventional space group *I*2/*a*, which they selected in order to maintain the relationship with the trigonal cell of quartz, such that $a_{mog} = 2a_{qtz} + b_{qtz}$, $b_{mog} = b_{qtz}$, and $c_{mog} = 2c_{qtz}$. X-ray structure analysis of natural moganite is challenging, because no crystals suitable for single-crystal X-ray diffraction studies have been discovered. More-

* E-mail: heaney@geosc.psu.edu

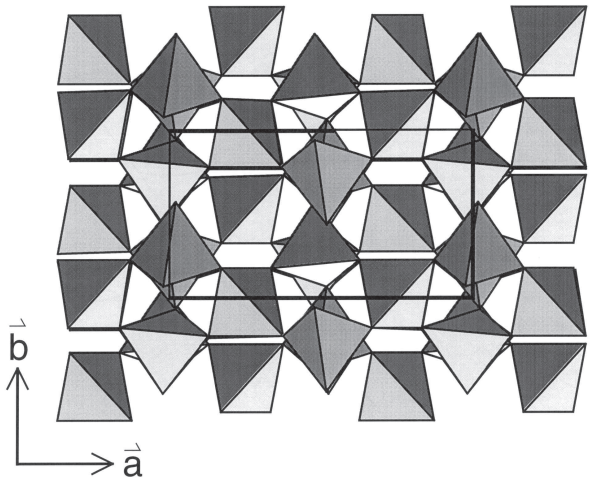

FIGURE 1. A projection of the structure of α-moganite along *c*.

over, peaks in X-ray powder diffraction patterns exhibit full widths at half-maxima of ~0.4 °2θ; this broadening arises from several factors: (1) Effective particle sizes fall well below 1 μm; (2) Structural disorder is rampant; (3) Moganite is usually intergrown with its structural sister, quartz; and (4) X-ray diffraction peaks even in pure moganite suffer from severe overlap, since the room-temperature structure is pseudo-orthorhombic and the lattice is pseudo-hexagonal. As a result, Miehe and Graetsch (1992) observed that their unconstrained refinement of moganite was troubled by a few unreasonable Si-O distances, and their reported structure parameters for moganite were derived from a distance least squares analysis without additional refinement of atom positions.

Nevertheless, the general moganite structure as presented by Miehe and Graetsch (1992) is widely accepted, and scientists have discovered isomorphous structures in other systems. For example, cristobalite- and quartz-type phosphorus oxynitride (PON) can be converted to a moganite analog after treatment at 850 °C and 2.5 GPa (Chateau et al. 1999). In addition, Haines et al. (1999) recognized that the structure of beryllium hydride (BeH_2) is topologically identical with that of moganite. In their solution and refinement of BeH_2, however, Smith et al. (1988) found that an orthorhombic space group (*Ibam*) rather than a monoclinic space group yielded the most reasonable structure. As noted by Miehe and Graetsch (1992), the *I*2/*a* modification of SiO_2-moganite is a subgroup of the *Imab* (=*Ibam*) aristotype, but these authors were unable to detect evidence for a symmetry-changing transition from *I*2/*a* to *Imab* using Guinier-Lenné diffraction photographs when samples were heated to 900 °C (1173 K).

We have used temperature-resolved synchrotron X-ray diffraction in conjunction with Rietveld refinement to obtain high quality measurements of the thermal expansion of moganite from 100 K to 1354 K, and our results provide strong support for a displacive *I*2/*a* to *Imab* transition from an α- to a β-moganite polymorph at approximately 570 K. As with Miehe and Graetsch (1992), peak overlap prevented us from refining reasonable atom positions for the structure at each of these temperatures. Nevertheless, our analysis of neutron diffraction data in which low *d*-spacing diffraction peaks are well represented has provided unconstrained atom parameters for the room-temperature structure of α-moganite.

EXPERIMENTAL METHODS

Data collection

Diffraction data were collected using the white, unconsolidated powders that form rinds around chert nodules from the Mogán D formation near the town of Mogán, Gran Canaria, Spain; these rinds appear to be forming as a modern alteration product at the contact between the translucent chert cores and the ferric feldspars that comprise much of the host ignimbrite. Examination of these powders by transmission electron microscopy reveals that individual particles consist of stacked laths measuring ~10 nm in width and 100 nm or more in length.

Room temperature time-of-flight neutron diffraction experiments were performed at the Manuel Lujan, Jr. Neutron Scattering Center at the Los Alamos National Laboratory. The sample was loaded into a V capsule, and data were collected by four detector banks centered at ± 90° 2θ and ± 151°2θ on the high intensity powder diffractometer (HIPD). Variable temperature synchrotron X-ray diffraction data were collected at beam line X7B of the National Synchrotron Light Source (NSLS), Brookhaven National Laboratory (BNL). The wavelengths used were 0.9492 Å for the experiment at ~100 K and 0.937 Å for all other experiments, as calibrated with ZrO_2 and LaB_6 standards.

For the low-temperature run, a sample was placed within a 0.5 mm diameter quartz-glass capillary and cooled to 100 ± 5 K by an Oxford Cryosystems temperature controller using boiled liquid nitrogen. For the high temperature experiments, the sample was heated from 298 K to 1354 K at 3.5 K/min using a Blake Instruments furnace with a Pt-13% Rh coiled wire yoke encased in ZrO_2 cement (Brown et al. 1973). The temperature was varied with an Omega controller and monitored with a chromel-alumel thermocouple located ~2 mm from the specimen. The temperature gradient between the sample and the thermocouple was determined for the range 298 K to 1273 K by a variety of melting transitions and by the placement of an additional thermocouple in the sample position. The highly linear relationship between the observed and actual temperatures ($r^2 = 0.983$) allowed us to calculate a calibration curve with an estimated error of ± 5 K for a given temperature.

Intensities for the 100 K run were collected during a 3 minute exposure with a 20 × 40 cm Fuji imaging plate mounted perpendicular to the incoming beam at a distance of 217.2 mm. The exposed plate was scanned by a Fuji BAS2000 reader, which yielded a nominal pixel size of 0.1 × 0.1 mm^2 (2048 × 4096 pixels) and a dynamic range of 10^4. Additional details for this procedure are provided in Norby (1997). The 298 K to 1354 K diffraction profiles were collected as a series of 90 s exposures with a Mar345 full imaging plate detector. The temperature was increased continuously and measurements were obtained every ~12 K; due to down time for reading the detector plate, each exposure represents a temperature range of ~5 K. During each exposure, the sample was rotated through a 90° angle. Any preferred orientation of the powder should have

been eliminated through a combination of this specimen rotation and the full intensity integration of the diffraction rings, as obtained using the program Fit2D (Hammersley et al. 1996) with a polarization factor of 0.93.

Structure refinements

All refinements were performed with the General Structure Analysis System (GSAS) program of Larson and Von Dreele (2001). The starting parameters for the 100 K and the 298 K refinements were taken from Miehe and Graetsch (1992) for moganite and from Will et al. (1988) for quartz. The amount of quartz in the powders refined to values of 30 ± 2 wt% for the neutron diffraction sample and 5 ± 3 wt% for the high-temperature synchrotron X-ray diffraction sample; lattice parameters for quartz over the temperatures investigated were taken from Carpenter et al. (1998b) and not further refined. For moganite, we used the final refined structural parameters at 298 K as the starting parameters for the next highest temperature and continued this procedure systematically with increasing temperature. At the inferred transition to *Imab* symmetry, we calculated a starting orthorhombic structure by constraining Si-O bond lengths to 1.61 Å in the *Imab* space group using GSAS.

The refinement parameters included scale factors for quartz and moganite and 30 to 36 background terms in a linear interpolation function. Peak profiles in the neutron diffraction data were based on the profile convolution function of Von Dreele et al. (1982), whereas those for the X-ray intensities were modeled by a pseudovoigt profile function as parametrized by Thompson et al. (1987) with asymmetry corrections by Finger et al. (1994) and microstrain anisotropic broadening terms by Stephens (1999). After convergence of these parameters, unit-cell dimensions, atom positions, and isotropic temperature factors were refined.

The room temperature refinement using neutron diffraction data yielded a reasonable structure with Marquardt damping but no bond distance or angle restraints. By contrast, refinements at low and high temperatures based only on synchrotron X-ray diffraction data consistently generated unreasonable bond distances (e.g., Si1-O2 = 1.65 Å and Si2-O1 = 1.56 Å). Therefore, all refinements using synchrotron X-ray diffraction data included 8 bond distance constraints that set all Si-O bond lengths equal to 1.61 Å. We attribute the superior quality of the TOF neutron diffraction refinement to the greater representation of low *d*-spacing diffraction data (1434 reflections with a lower *d*-spacing limit of 0.55 Å in the TOF neutron data set vs. 163 reflections with a limit of 1.14 Å in the synchrotron X-ray data set).

Estimations of error

In our Rietveld analyses using synchrotron X-ray diffraction data, the final χ^2 values ranged from 0.10 to 3.17, with half of the χ^2 values below 1.00. The reduced χ^2 is calculated by GSAS as $\chi^2 = M/(N_{obs}–N_{var})$, where N_{obs} is the number of observed intensities and N_{var} is the number of refined variables. M is the function minimized during the refinement and is defined as $M = \Sigma w(I_o–I_c)^2$, where I_o and I_c are the observed and calculated intensities at a given value of 2θ and the weighting factor w is equal to the inverse of the square of the estimated standard deviation [i.e., $w = 1/(\text{e.s.d.})^2$] (Larson and Von Dreele 2001). In our datasets, the esd for a given 2θ was arbitrarily calculated as the square root of the intensity. Because an amorphous component contributed very high background intensities to our patterns, the calculated e.s.d. values for our patterns were unreasonably large. Consequently, the weighting factors w were unreasonably low, generating values for χ^2 that consistently fell below unity.

Our inspection of the variation in the estimated standard deviation as a function of the scattering angle revealed no systematic dependence on 2θ. Consequently, the minimization calculations performed by GSAS were not biased by the unrealistic e.s.d. values. As a result, the final χ^2 values calculated during our analyses of the synchtrotron X-ray diffraction data are meaningful as relative measures of the goodness of fit, albeit not as absolute measures. However, the reasonable bond distances and the low values for R_{wp} and R_{Bragg} provided independent measures of the accuracy of the final refined structure.

As is often the case, the standard deviations calculated by GSAS for the lattice parameters are lower than the true errors, which are revealed by the scatter in the refined values as a function of temperature (Post and Bish 1989). We present the errors calculated by GSAS in the tables and figures of this paper with the understanding that the actual errors may be more than an order of magnitude higher than the calculated deviations.

Results and Discussion

Room-temperature refinement

The refinement parameters for the structure of moganite at room temperature based on TOF neutron diffraction data are listed in Table 1. Atom positions and selected bond distances and angles are reproduced in Tables 2 and 3. The close fit between the intensities generated by our final refined structures and the observed X-ray and neutron diffraction intensities is evident in Figure 2. Our results are in good agreement with the structure reported by Miehe and Graetsch (1992), including their assignment of space group *I*2/*a* to the room temperature modification. The aristotypic space group *Imab* requires that all *hk*0 reflections with *h*, *k* odd are absent due to *a* and *b* glides

Table 1. Parameters for neutron diffraction refinement of α-moganite at 298 K

Chemical formula	SiO_2
Crystal system	Monoclinic
Space group	*I*2/*a*
Unit cell	
a (Å)	8.7371(6)
b (Å)	4.8692(3)
c (Å)	10.7217(7)
β (°)	90.193(9)
V (Å^3)	456.12(5)
Refinement	
No. of data points	4355
No. of reflections	1434
Diffraction range	
TOF	2765 to 24 000 μs
d-spacing	0.55 to 4.8 Å
No. of variables	64
R_{Bragg}	0.0475
R_{wp}	0.0210
χ^2	3.801

TABLE 2. Atomic coordinates and isotropic temperature factors from neutron refinement for α-moganite at 298 K in *I*2/*a*

Atom	*x*	*y*	*z*	$U_{iso} \times 100$ (Å^2)
Si1	1/4	0.9726(11)	0	0.97(4)
Si2	0.0103(3)	0.2486(7)	0.1682(4)	1.10(2)
O1	0.9781(3)	0.0644(5)	0.2878(2)	1.48(2)
O2	0.1678(3)	0.1708(5)	0.1002(3)	1.72(2)
O3	0.8703(3)	0.2296(5)	0.0675(3)	1.89(2)

TABLE 3. Selected bond lengths and angles in α-moganite from neutron refinement at 298 K

Bond	Bond Length (Å)
Si1-O2	1.614(4)
Si1-O3	1.610(4)
Si2-O1	1.590(5)
Si2-O1	1.612(4)
Si2-O2	1.605(4)
Si2-O3	1.632(4)
Atoms	**Angle (°)**
O2-Si1-O2	106.6(4)
O2-Si1-O3	111.9(1)
O2-Si1-O3	111.0(2)
O3-Si1-O3	104.6(4)
O1-Si2-O1	108.3(2)
O1-Si2-O2	112.8(2)
O1-Si2-O3	111.5(2)
O1-Si2-O2	107.8(2)
O1-Si2-O3	107.1(2)
O2-Si2-O3	109.2(3)
Si2-O1-Si2	139.7(2)
Si1-O2-Si2	145.8(2)
Si1-O3-Si2	145.0(3)

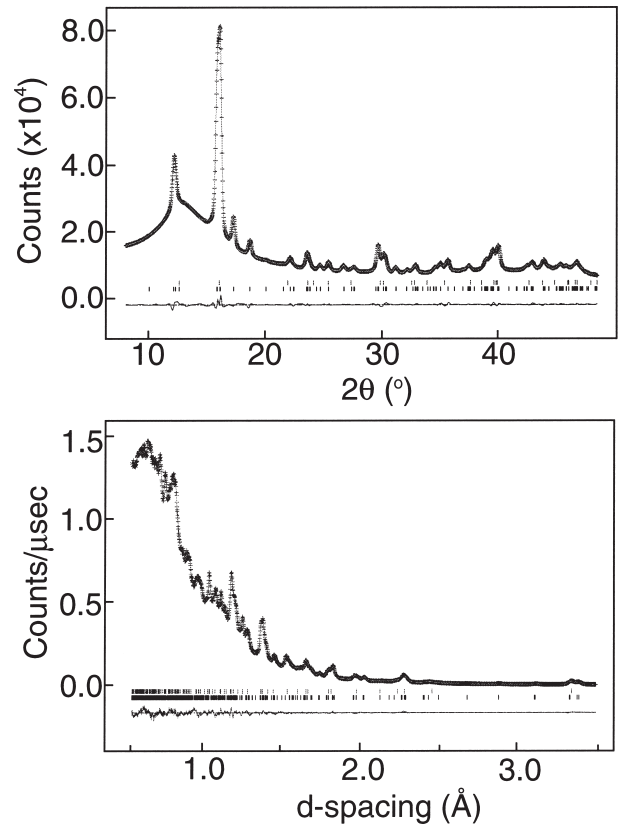

FIGURE 2. X-ray (top; λ = 0.937 Å) and neutron (bottom) powder diffraction patterns for α-moganite at room temperature. Rietveld analysis yields a close correspondence between the observed intensities (crosses) and calculated intensities (lines). Tick marks beneath patterns represent peak positions for quartz (top) and moganite (bottom). Difference curves are at bottoms of patterns.

parallel to (001). The strongest member of this class is the 310 reflection at 2.5014 Å, and, as is discussed below in the context of the heating experiments, the 310 reflection is unambiguously present in room temperature diffraction patterns of moganite. This observation eliminates *Imab* as a possible space group for moganite at 298 K. Interestingly, Chateau et al. (1999) were unable to distinguish the 310 peak from background intensity in their study of highly crystalline moganite-like PON. Nevertheless, they selected *I*2/*a* as the proper symmetry on the basis of their refinements in both monoclinic and orthorhombic space groups.

It is possible that silica moganite belongs to a lower order space group, such as triclinic $I\bar{1}$. Our refinements in this space group led to lattice parameters that differed from their monoclinic counterparts by less than 0.2% with a comparable goodness of fit. However, close inspection of the room-temperature neutron and synchrotron X-ray diffraction patterns revealed no violations of the conditions imposed by the *a* glide parallel to (010) in *I*2/*a* (i.e., *h* even for all *h*0*l* reflections). Consequently, *I*2/*a* appears to be the most likely space group symmetry for room-temperature moganite.

Lattice variation with temperature

The synchrotron powder X-ray diffraction patterns of moganite with increasing temperature revealed a subtle shift in peak positions at ~570 K (Fig. 3a) and a dramatic decrease in background intensity at ~700 K (Fig. 3b). The existence of a reversible phase transition at or near 570 K is strongly supported by the variation observed in individual unit-cell parameters over the temperature range 100 K to 1354 K (Fig. 4 and Table 4). Specifically, *a* increased with a linear expansion coefficient of 2.89×10^{-5} K^{-1} on heating to 569 K; above this point, *a* remained constant within error. The *b* parameter increased continuously over the experimental temperature range, but the linear expansion coefficient decreased from 1.42×10^{-5} K^{-1} to 1.13×10^{-5} K^{-1} above 569 K. The *c* axis length varied least among the cell parameters; we believe that most of the scatter between 350 K and 1200 K is an indication of the true error and that *c* is virtually constant over most of the temperature range analyzed. As a result of these changes in axial expansions, the volume also experiences a decrease in its linear expansion coefficient from 5.08×10^{-5} K^{-1} between 100 K and 569 K to 1.02×10^{-5} K^{-1} between 569 K and 1354 K.

The cell angle β is the most direct measure of monoclinicity and could serve as an order parameter (Q) for an *I*2/*a* –*Imab* transition. However, β refined less robustly below 569 K than did the cell edge lengths; the intentional introduction of small perturbations of other refinement parameters induced variations of ±0.05° in the refined values of β. We attribute this instability to the closeness of β to the orthorhombic value of 90°. Nev-

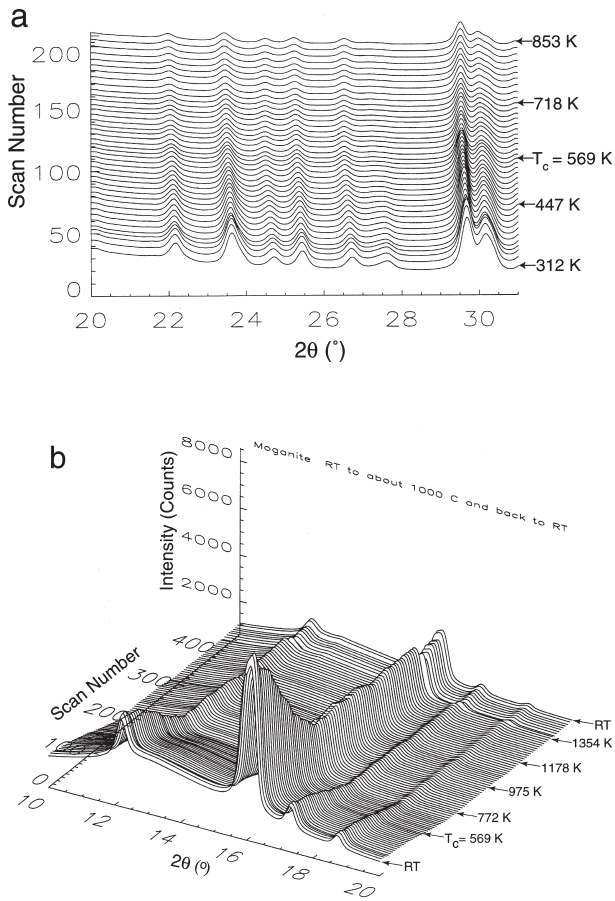

FIGURE 3. Evolution of synchrotron X-ray diffraction patterns revealing subtle shifts in peak positions (**a**) and a sharp decrease in background intensity (**b**) with increasing temperature (λ = 0.937 Å).

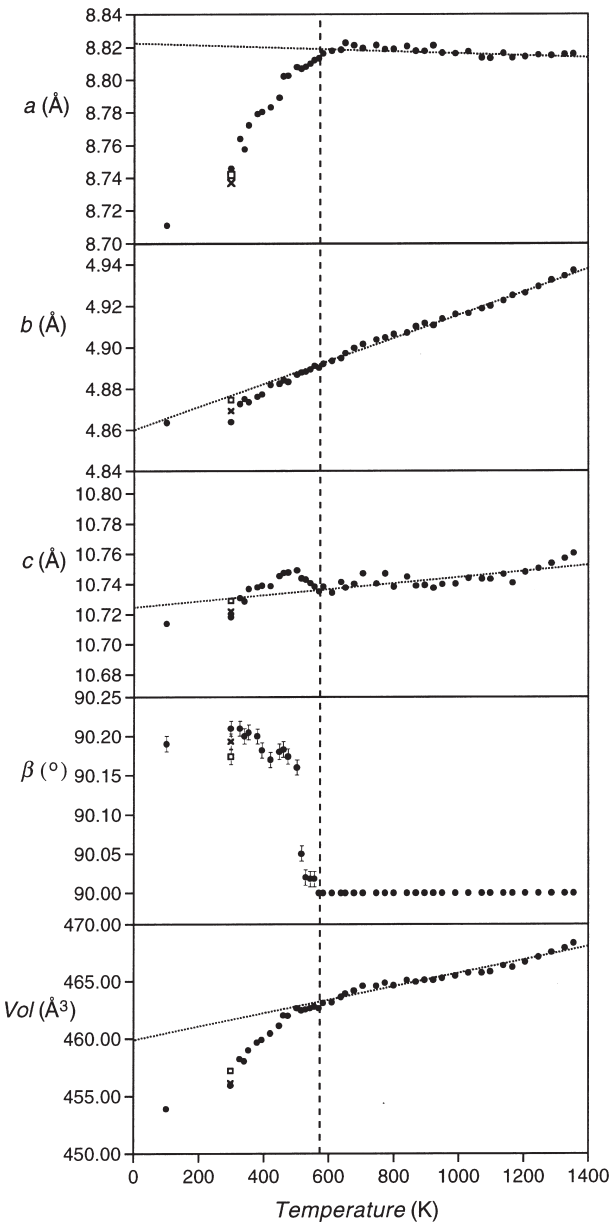

FIGURE 4. Variation of the unit-cell parameters and volume as a function of temperature. Vertical dashed line represents proposed α-β moganite transition point at ~570 K. Dotted lines in each graph represent lattice values that are derived from a least-squares fit of β-moganite parameters and extrapolated into the stability field for α-moganite. Symbols: circle = Synchrotron XRD during heating; box = Synchrotron XRD after cooling to 298 K; cross = Neutron diffraction at 298 K.

ertheless, the refinements between 525 K and 569 K appeared quite robust, and these analyses yielded values of ~90.02° for β. Thus, the overall decrease in β with increased temperature is consistent with a transition near 569 K from monoclinic to orthorhombic symmetry. Moreover, refinement of the 555 K data set using the *I*2/*a* structure ($\chi^2 = 1.102$) yielded a slightly better refinement than with the *Imab* structure ($\chi^2 = 1.187$). On the other hand, the run at 569 K produced a slightly worse result in *I*2/*a* ($\chi^2 = 0.98$) than in *Imab* ($\chi^2 = 0.87$). Because of the additional parameters required for the lower symmetry structure, these differences in χ^2 may not be significant. Calorimetric studies are required to locate the critical point with greater precision.

That the high temperature structure belongs to space group *Imab* is supported by many lines of evidence. As has been described previously (Miehe and Graetsch 1992; O'Keeffe and Hyde 1996; Haines et al. 1999), the space groups *I*2/*a* and *Imab* share a subgroup-supergroup relationship, and the mechanism responsible for the transition in moganite can be effected by a simple rotation of rigid tetrahedra about [010] (Fig. 5). This tetrahedral tilting mechanism can be quantified simply as the angle φ between the **a** axis and the projected edge of the Si1 tetrahedron on the (010) plane. The angle φ may be calculated from the relation

$$\tan \phi = \frac{|\Delta z|\,|c| \sin \beta}{|\Delta x|\,|a| - |\Delta z|\,|c| \cos \beta} \quad (1)$$

TABLE 4. Unit-cell parameters for moganite as a function of temperature based on synchrotron XRD

T (K)	*a* (Å)	*b* (Å)	*c* (Å)	β (°)	Vol. (Å^3)
100	8.711(1)	4.8636(6)	10.714(1)	90.19(1)	453.9(1)
298	8.7458(6)	4.8639(3)	10.7184(8)	90.21(1)	455.95(3)
325	8.7640(8)	4.8726(4)	10.7308(8)	90.21(1)	458.24(7)
339	8.7577(9)	4.8751(4)	10.7287(11)	90.20(1)	458.06(9)
352	8.7722(3)	4.8735(2)	10.7369(4)	90.21(1)	459.01(3)
379	8.7791(7)	4.8762(3)	10.7380(7)	90.20(1)	459.67(6)
393	8.7805(4)	4.8773(2)	10.7392(4)	90.18(1)	459.91(3)
420	8.7833(5)	4.8818(3)	10.7388(6)	90.17(1)	460.46(4)
447	8.7892(5)	4.8825(3)	10.7455(6)	90.18(1)	461.12(4)
460	8.8021(8)	4.8841(4)	10.7476(8)	90.18(1)	462.04(7)
474	8.8025(4)	4.8834(2)	10.7479(5)	90.17(1)	462.01(3)
501	8.8078(4)	4.8868(2)	10.7493(5)	90.16(1)	462.67(3)
515	8.8068(9)	4.8879(4)	10.7439(10)	90.05(1)	462.49(8)
528	8.8081(9)	4.8883(4)	10.7432(10)	90.02(2)	462.57(8)
542	8.8099(8)	4.8894(4)	10.7408(9)	90.02(1)	462.67(8)
555	8.8122(8)	4.8910(4)	10.7385(8)	90.02(1)	462.83(7)
569	8.8133(3)	4.8901(2)	10.7353(4)	90	462.67(3)
582	8.8162(9)	4.8920(4)	10.7385(10)	90	463.14(9)
609	8.8179(8)	4.8935(4)	10.7344(10)	90	463.19(8)
637	8.8185(6)	4.8948(3)	10.7416(8)	90	463.66(3)
650	8.8226(7)	4.8972(4)	10.7378(9)	90	463.94(8)
677	8.8211(8)	4.8998(4)	10.7403(9)	90	464.21(8)
704	8.8194(7)	4.9017(3)	10.7473(10)	90	464.61(3)
745	8.8213(8)	4.9038(4)	10.7405(9)	90	464.61(8)
772	8.8188(7)	4.9049(3)	10.7472(10)	90	464.87(3)
799	8.8189(8)	4.9065(4)	10.7384(10)	90	464.65(8)
840	8.8206(7)	4.9072(3)	10.7451(9)	90	465.10(3)
867	8.8178(8)	4.9102(4)	10.7389(10)	90	464.97(9)
894	8.8176(8)	4.9117(4)	10.7394(11)	90	465.12(9)
921	8.8210(11)	4.9107(6)	10.7376(15)	90	465.12(12)
948	8.8166(8)	4.9138(4)	10.7401(10)	90	465.29(8)
989	8.8162(8)	4.9160(4)	10.7404(11)	90	465.49(9)
1029	8.8174(7)	4.9165(3)	10.7442(11)	90	465.76(3)
1070	8.8135(9)	4.9188(4)	10.7437(12)	90	465.76(9)
1097	8.8133(9)	4.9201(4)	10.7435(12)	90	465.86(9)
1137	8.8163(7)	4.9226(3)	10.7468(11)	90	466.40(3)
1165	8.8136(9)	4.9252(5)	10.7411(13)	90	466.26(10)
1205	8.8143(11)	4.9264(6)	10.7482(15)	90	466.72(12)
1246	8.8153(8)	4.9294(4)	10.7505(12)	90	467.15(3)
1286	8.8149(5)	4.9325(3)	10.7538(6)	90	467.57(4)
1327	8.8156(5)	4.9345(3)	10.7570(6)	90	467.94(4)
1354	8.8159(9)	4.9371(5)	10.7605(14)	90	468.35(11)
298	8.7419(4)	4.8746(2)	10.7290(5)	90.17(1)	457.20(4)

where Δz = O2z – O3z and Δx = O3x – O2x. In moganite, β is so nearly equal to 90° that the formula effectively reduces to

$$\tan \phi = \frac{|\Delta z|\ |c|}{|\Delta x|\ |a|} \quad (2)$$

As noted above, our refined atom positions at high temperatures required temperature factor and bond distance restraints with Si-O set to 1.61 Å. Nevertheless, we expect that our refined high-temperature structure is reasonably accurate, and we can compare the value from our room temperature refinement using TOF neutron diffraction data with our synchrotron X-ray diffraction result just below the transition temperature. This analysis reveals that φ decreases from 11.8° at room temperature to 1.5° at 555 K, as is consistent with the proposed tetrahedral tilting mechanism.

The structural response of a tetrahedral rotation about [010] is an expansion along the **a** axis. Consequently, if tetrahedral tilting is the driving mechanism behind the transition in symmetry from *I*2/*a* to *Imab*, then one would expect the **a** axis to increase steadily from 100 K to the transition temperature, as is observed. Once the tetrahedra are fully rotated such that φ = 0°

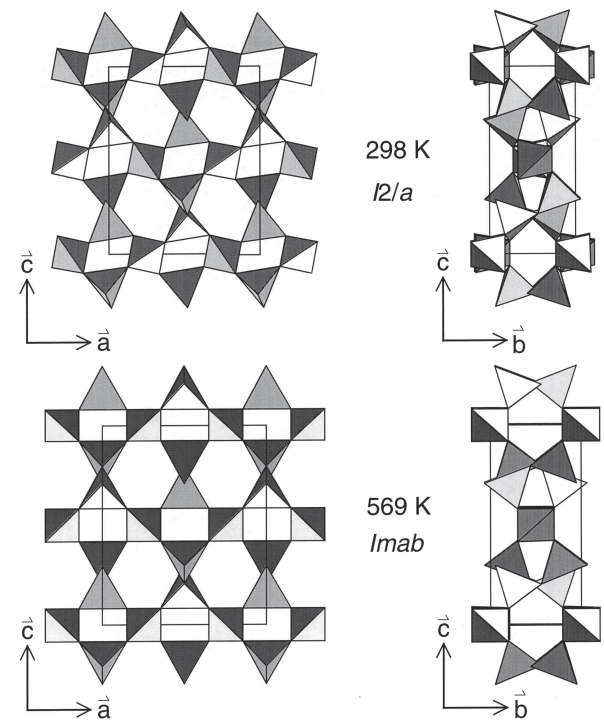

FIGURE 5. Projections of the structures of α-moganite **(top)** and β-moganite **(bottom)** on to the (010) plane **(left)** and the (100) plane **(right)**. The transformation from monoclinic to orthorhombic symmetry is effected by rotations of tetrahedra about the [010] axis.

and β = 90°, orthorhombic symmetry is achieved and additional expansion along **a** ceases. The plateau-like behavior of the thermal expansion of the **a** axis at the transition (Fig. 4) is fully consistent with this mechanism.

Lastly, the attainment of *Imab* symmetry in β-moganite is supported by the gradual disappearance of the 310 peak at the transition temperature (Fig. 6). As previously described, a small but distinct 310 peak was visible in the synchrotron X-ray diffraction pattern at room temperature, but it was no longer discernible at 569 K. When the sample was cooled to room temperature again, however, the 310 peak could be observed with even greater clarity as a result of a diminished background contribution. The reappearance of the 310 peak and the recovery of the lattice parameters to their original values after cycling back to room temperature (Fig. 4) indicate that the transition from α- to β-moganite is reversible. The results of our constrained refinement of β-moganite in space group *Imab* at 1354 K are presented in Table 5.

Character of the transition

The inversion from β-moganite with space group *Imab* to α-moganite with space group *I*2/*a* is associated with the Brillouin zone center. As the change in Laue class involves a transition from *mmm* to 2/*m*, the active representation is B_{2g} and the symmetry-breaking strain is e_{13}. The remaining A_g strains are e_{11}, e_{22}, and e_{33}, which are non-symmetry-breaking;

TABLE 5. Atomic coordinates for β-moganite at 1354 K in space group *Imab*

Atom	x	y	z
Si1	1/4	0	0
Si2	0	0.2255(6)	0.1701(3)
O1	0	0.0416(7)	0.2935(4)
O2	0.1471(3)	0.2007(6)	0.0824(5)

Notes: (1) Refined with 8 Si-O bonds constrained to 1.61 Å; (2) Refined with U_{iso} constrained to 0.03 Å^2 for all atoms; (3) Referenced to origin at $2/m_{100}$. To convert to origin at $\bar{1}$, add 1/4 1/4 1/4 to xyz coordinates.

e_{12} and e_{23} are equal to zero. For the orthorhombic to monoclinic transformation, these strains are calculated as follows:

$$e_{11} = \frac{a}{a_0} - 1 \quad (3) \qquad e_{22} = \frac{b}{b_0} - 1 \quad (4)$$

$$e_{33} = \frac{c}{c_0}\sin\beta - 1 \quad (5) \qquad e_{13} = \frac{1}{2}\left(\frac{c}{c_0}\cos\beta\right) \quad (6)$$

where the subscript 0 denotes the value extrapolated from the observed strain in β-moganite to the stability field for α-moganite (Carpenter et al. 1998a, Carpenter and Salje 1998). Similarly, the volume strain V_s can be calculated from the relation

$$V_s = \frac{V}{V_0} - 1. \quad (7)$$

The high degree of scatter in our refined values of the *c* and β unit-cell parameters precluded a meaningful treatment of the variation of the e_{33} and e_{13} strains as a function of temperature. However, an analysis of the evolution of the e_{11}, e_{22}, and volume strains as a function of temperature reveals a continuous and linear approach to zero near T_c (Fig. 7). These results indicate that the volume strain V_s and the non-symmetry-breaking strains e_{nsb} vary as the square of the order parameter, so that the α-β moganite transition is second-order in character ($Q^2 \propto T \propto V_s \propto e_{nsb}$). This result is consistent with the continuous variation of the cell volume across the transition.

The volume strain associated with the moganite transformation is low in comparison with the well-known displacive transitions in quartz and cristobalite. The value of V_s at $T/T_c = 0.5$ is ~1% in moganite. By comparison, the half-transition volume strain for the $P6_222$–$P3_221$ transition in quartz is ~4% (Carpenter et al. 1998b), and that for the $Fd\bar{3}m$ – $P4_12_12$ transition in cristobalite is slightly greater than 5% (Schmahl et al. 1992). The degree of structural distortion in moganite is more comparable to the ~1% volume strain generated by the non-symmetry-breaking transition at 465 °C in hexagonal tridymite documented by de Dombal and Carpenter (1993).

Significance of elevated background intensity

An examination of the x-ray diffraction patterns produced by the moganite-rich rinds reveals a dramatic and irreversible decrease in background intensity with increasing temperature (Fig. 3b). The cause of this extraneous scattering remains uncertain, but two possibilities may be postulated: intergrowth of disordered opal-CT and/or local structural disorder in the moganite structure.

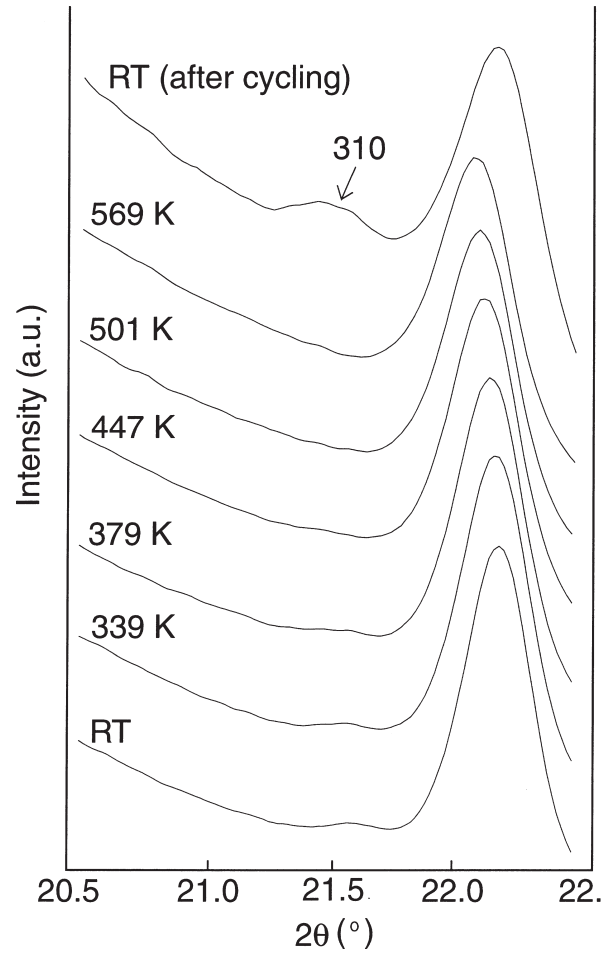

FIGURE 6. Synchrotron X-ray diffraction reveals that the intensity of the 310 peak diminishes to zero as the transition temperature is approached. Upon cooling to room temperature, the peak reappears (λ = 0.937 Å).

Opaline intergrowths. The *d*-spacing of the maximum intensity of the broad background peak occurs at ~4.13 Å, and the position of this maximum does not vary appreciably with temperature. This *d*-spacing exceeds the basal spacings of low cristobalite (4.04 Å) and low tridymite (4.10 Å), but it closely matches the *d*-spacing of ~4.12 Å observed in the most strongly disordered opal-CT (Graetsch 1994). After the moganite powder was heated to 700 K in a little less than 2 hours, the background intensity at 4.13 Å diminished to its minimum value (Fig. 3b). Because the moganite used in this study precipitated during low-temperature alteration processes, the inclusion of an opaline phase within the chert-like nodules is geologically plausible. Moreover, the radial distribution function calculated from the background intensity reveals strong peaks at 1.6 Å and 2.6 Å, which correspond to Si-O and O-O distances, respectively. Consequently, the high background may derive from an amorphous, opaline phase. If so, then the decrease in background intensity with higher temperature may be associated

with the loss of H_2O or with the conversion of opal-CT to opal-C. However, the kinetics of these reactions as observed in our experiments do not exactly match rates reported elsewhere. Differential thermal gravimetric studies of opal-C reveal that most molecular water is lost at 200 °C (473 K) in less than 0.5 hours when heated at 8 K/min (Graetsch et al. 1985), and Miehe and Graetsch (1992) observed the transformation of moganite to cristobalite beginning at 900 °C (1173 K).

Chain kinking. Alternatively, the high background intensity may be attributed to local structural defects within the moganite structure that anneal with increasing temperature. Twins in α-moganite presumably are abundant, as growth twins will obey the same law that controls inversion twinning at the β- to α-moganite transition, specifically the loss of a mirror plane along (010). However, the contribution of these twins to background intensity must disappear at the transition temperature of 569 K, which is more than 100 K below the temperature at which the background achieves its minimum. Similarly, it is unlikely that α-β quartz-like transition modes confer a heightened background intensity. As described by Van Goethem et al. (1977), the Dauphiné twin boundaries found in α-quartz are not compatible with the structure of Brazil twin boundaries. Since moganite is Brazil-twinned at the unit-cell scale, we do not expect to observe behaviors attributable to the α-β quartz transformation at 846 K, and nothing in the evolution of the lattice parameters or background intensities contradicts this inference.

On the other hand, Haines et al. (1999) have argued that moganite-like crystal structures may be susceptible to conformational disorder within the tetrahedral chains parallel to **b**. Although BeH_2 is topologically identical to moganite, the distortion of the tetrahedral chains along **b** differs from that observed in SiO_2 and PON moganite; BeH_2 chains kink in a sympathetic fashion, creating large elongate tunnels that run parallel to **a**, whereas an antipathetic kinking in SiO_2 and PON moganite generates smaller and more equant tunnels along **a** (Fig. 8). It is possible that metastable BeH_2-like regions exist within silica moganite, giving rise to a heightened background intensity. It seems quite reasonable that these defects would anneal at the temperatures and timescales that characterized our experiments. The transformation from the BeH_2 to the SiO_2 (or PON) chain conformation is achieved by tetrahedral rotations that do not break bonds, and overall symmetry remains unchanged. Moreover, the continuous increase in the length of the *b* axis with increasing temperature (Fig. 4) strongly suggests that the tetrahedral [010] chains are gradually unkinking in response to polyhedral rotations about the **a** axis. At a sufficiently high temperature, these chains might achieve the perfectly straight backbone that characterizes the [100] chains in β-quartz. Confirmation of these possibilities awaits high resolution structural analyses of moganite at high temperatures over both long- and short-length scales.

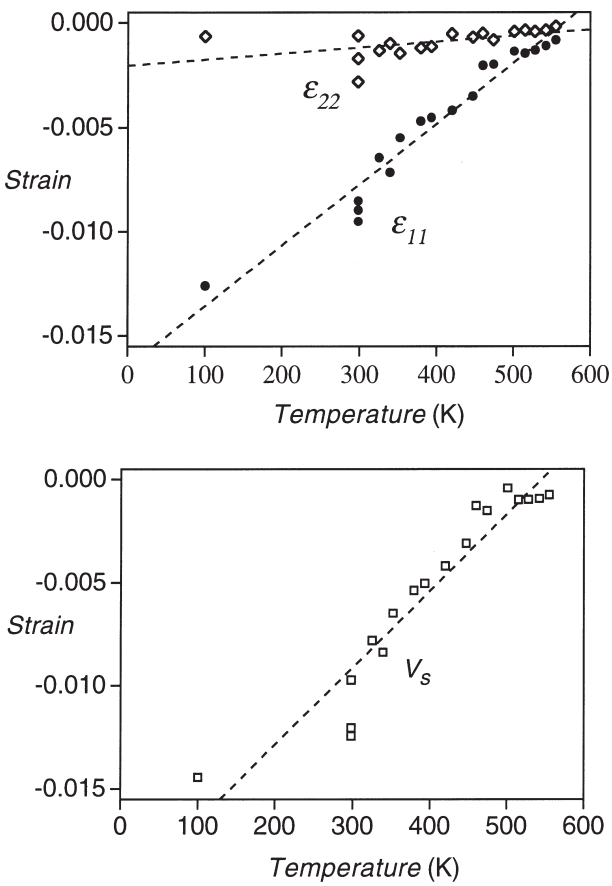

FIGURE 7. Variation in ε_{11} and ε_{22} strains (**top**) and volume strain (**bottom**) as a function of temperature.

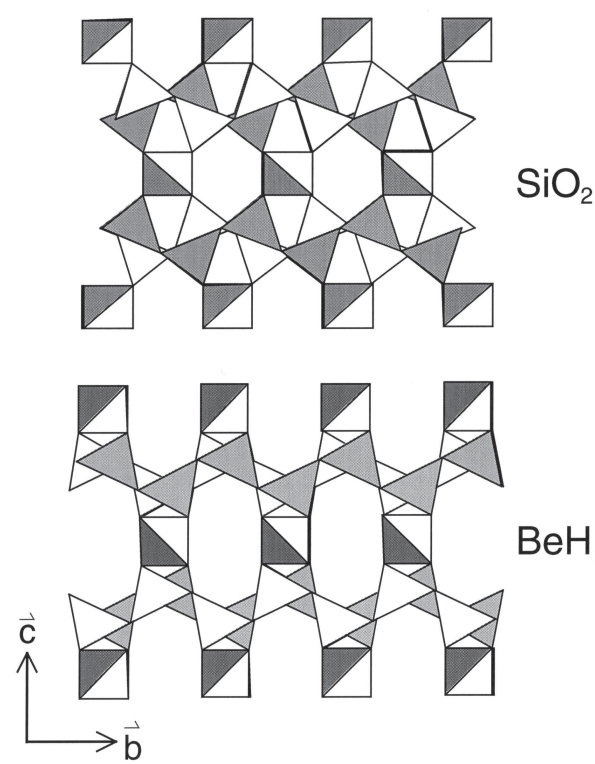

FIGURE 8. Projections of the structures of β-moganite and BeH_2 along the **a** axis. The frameworks are topologically identical but differ in the configuration of the [010] chains.

ACKNOWLEDGMENTS

We thank J. Hanson for his help with the collection and processing of the synchrotron X-ray powder diffraction data, and R. Von Dreele for his assistance with the neutron diffraction experiments and the data analysis using GSAS. We are grateful for comments from M. Henderson, M. Fleet, and an anonymous reviewer. This work was supported by National Science Foundation grant no. EAR-0073862. Synchrotron X-ray diffraction was carried out at the National Synchrotron Light Source (NSLS), Brookhaven National Laboratory, and neutron diffraction was performed at the Manuel Lujan, Jr. Neutron Scattering Center (MLNSC), Los Alamos National Laboratory. Research at Brookhaven was supported under contract DE-AC02-98CH10886 with the U.S. Department of Energy by its Division of Chemical Sciences, Office of Basic Energy Research.

REFERENCES CITED

Brown, G.E., Sueno, S., and Prewitt, C.T. (1973) A new single-crystal heater for the precession camera and four-circle diffractometer. American Mineralogist, 58, 698–704.

Carpenter, M.A. and Salje, E.K.H. (1998) Elastic anomalies in minerals due to structural phase transitions. European Journal of Mineralogy, 10, 693–812.

Carpenter, M.A., Salje, E.K.H., and Graeme-Barber, A. (1998a) Spontaneous strain as a determinant of thermodynamic properties for phase transitions in minerals. European Journal of Mineralogy, 10, 621–691.

Carpenter, M.A., Salje, E.K.H., Graeme-Barber, A., Wruck, B., Dove, M.T., and Knight, K.S. (1998b) Calibration of excess thermodynamic properties and elastic constant variations associated with the $\alpha \leftrightarrow \beta$ phase transition in quartz. American Mineralogist, 83, 2–22.

Chateau, C., Haines, J., Léger, J.-M., LeSauze, A., and Marchand, R. (1999) A moganite-type phase in the silica analog phosphorus oxynitride. American Mineralogist, 84, 207–210.

de Dombal, R.F. and Carpenter, M.A. (1993) High-temperature phase transitions in Steinbach tridymite. European Journal of Mineralogy, 5, 607–622.

Dove, M.T., Trachenko, K.O., Tucker, M.G., and Keen, D.A. (2000) Rigid unit modes in framework structures: theory, experiment and applications. In S.A.T. Redfern and M.A. Carpenter, Eds., Transformation Processes In Minerals, 39, 1–33. Reviews in Mineralogy and Geochemistry, Mineralogical Society of America, Washington, D.C.

Finger, L.W., Cox, D.E., and Jephcoat, A.P. (1994) A correction for powder diffraction peak asymmetry due to axial divergence. Journal of Applied Crystallography, 27, 892–900.

Flörke, O.W., Jones, J.B., and Schmincke, H.-U. (1976) A new microcrystalline silica from Gran Canaria. Zeitschrift für Kristallographie, 143, 156–165.

Flörke, O.W., Flörke, U., and Giese, U. (1984) Moganite: a new microcrystalline silica-mineral. Neues Jahrbuch für Mineralogie. Abhandlungen, 149, 325–336.

Fournier, R.O. (1977) Chemical geothermometers and mixing models for geothermal systems. Geothermics, 5, 41–51.

Fournier, R.O. and Rowe, J.J. (1966) Estimation of underground temperatures from the silica content of water from hot springs and wet-steam wells. American Journal of Science, 264, 685–697.

Gíslason, S.R., Heaney, P.J., Oelkers, E.H., and Schott, J. (1997) Kinetic and thermodynamic properties of moganite, a novel silica polymorph. Geochimica et Cosmochimica Acta, 61, 1193–1204.

Graetsch, H. (1994) Structural characteristics of opaline and microcrystalline silica minerals. In P.J. Heaney, C.T. Prewitt, and G.V. Gibbs, Eds., Silica: physical behavior, geochemistry, and materials applications, 29, 209–232. Reviews in Mineralogy, Mineralogical Society of America, Washington, D.C.

Graetsch, H., Flörke, O.W., and Miehe, G. (1985) The nature of water in chalcedony and opal-C from Brazilian agate geodes. Physics and Chemistry of Minerals, 12, 300–306.

Haines, J., Chateau, C., Léger, J.M., Le Sauze, A., Diot, N., Marchand, R., and Hull, S. (1999) Crystal structure of moganite-type phosphorus oxynitride; relationship to other twinned-quartz-based structures. Acta Crystallographica, B55, 677–682.

Hammersley, A.P., Svensson S.O., Hanfland M., Fitch A.N., and Hausermann D. (1996) Two-dimensional detector software: From real detector to idealised image or two-theta scan. High Pressure Research, 14, 235–248.

Heaney, P.J. (1994) Structure and chemistry of the low-pressure silica polymorphs. In P.J. Heaney, C.T. Prewitt, and G.V. Gibbs, Eds., Silica: physical behavior, geochemistry, and materials applications, 29, 1–40. Reviews in Mineralogy, Mineralogical Society of America, Washington, D.C.

———(1995) Moganite as an indicator for vanished evaporites: A testament reborn? Journal of Sedimentary Research, A65, 633–638.

Heaney, P.J. and Post, J.E. (1992) The widespread distribution of a novel silica polymorph in microcrystalline quartz varieties. Science, 255, 441–443.

Larson, A.C. and Von Dreele, R.B. (2001) GSAS-General Structure Analysis System. Los Alamos National Laboratory Report No. LAUR 86–748.

Miehe, G. and Graetsch, H. (1992) Crystal structure of moganite: A new structure type for silica. European Journal of Mineralogy, 4, 693–706.

Miehe, G., Graetsch, H., Flörke, O.W., and Fuess, H. (1988) Die monokline Kristallstruktur des SiO_2-Minerals Moganit. Zeitschrift für Kristallographie, 182, 183–184. (Abstract)

Murashov, V.V. and Svishchev, I.M. (1998) Quartz family of silica polymorphs: comparative simulation study of quartz, moganite, and orthorhombic silica, and their phase transformations. Physical Review B, 57, 5639–5646.

Norby, P. (1997) Synchrotron powder diffraction using imaging plates: Crystal structure determination and Rietveld refinement. Journal of Applied Crystallography, 30, 21–30.

O'Keeffe, M. and Hyde, B.G. (1996) Crystal Structures. I. Patterns and Symmetry. Monograph 3, Mineralogical Society of America, Washington, D.C.

Petrovic, I., Heaney, P.J., and Navrotsky, A. (1996) Thermochemistry of the new silica polymorph moganite. Physics and Chemistry of Minerals, 23, 119–126.

Post, J.E. and Bish, D.L. (1989) Rietveld refinement of crystal structures using powder X-ray diffraction data. In D.L. Bish and J.E. Post, Eds., Modern Powder Diffraction, 20, 277–308. Reviews in Mineralogy, Mineralogical Society of America, Washington, D.C.

Raman, C.V. and Nedungadi, T.M.R. (1940) The α-β transformation of quartz. Nature, 145, 147.

Schmahl, W.W., Swainson, I.P., Dove, M.T., and Graeme-Barber, A. (1992) Landau free energy and order parameter behaviour of the α/β phase transition in cristobalite. Zeitschrift fur Kristallographie, 201, 125–145.

Smith, G.S., Johnson, Q.C., Smith, D.K., Cox, D.E., and Zalkin, A. (1988) The crystal and molecular structure of beryllium hydride. Solid State Communications, 67, 491–494.

Stephens, P.W. (1999) Phenomenological model of anisotropic peak broadening in powder diffraction. Journal of Applied Crystallography, 32, 281–289.

Thompson, P., Cox, D.E., and Hastings, J.B. (1987) Rietveld refinement of Debye-Scherrer synchrotron X-ray data from Al_2O_3. Journal of Applied Crystallography, 20, 79–83.

Van Goethem, L., van Landuyt, J., and Amelinckx, S. (1977) The α-β transition in amethyst quartz as studied by electron microscopy and diffraction. Physica Status Solidi, A41, 129–137.

Von Dreele, R.B., Jorgensen, J.D., and Windsor, C.G. (1982) Rietveld refinement with spallation neutron powder diffraction data. Journal of Applied Crystallography, 15, 581–589.

Will, G., Bellotto, M., Parrish, W., and Hart, M. (1988) Crystal structures of quartz and magnesium germanate by profile analysis of synchrotron-radiation high-resolution powder data. Journal of Applied Crystallography, 21, 182–191.

MANUSCRIPT RECEIVED MARCH 16, 2001
MANUSCRIPT ACCEPTED JULY 27, 2001
MANUSCRIPT HANDLED BY MICHAEL E. FLEET